Conjugate field and fluctuation-dissipation relation for the dynamic phase transition in the two-dimensional kinetic Ising model

D.T. Robb,[1, 2, *] P.A. Rikvold,[1, 3, 4] A. Berger,[5] and M.A. Novotny[6]

[1]*School of Computational Science, Florida State University, Tallahassee, Florida 32306, USA*

[2]*Department of Physics, Clarkson University, Potsdam, New York 13699, USA*

[3]*Center for Materials Research and Technology and Department of Physics, Florida State University, Tallahassee, Florida 32306-4350, USA*

[4]*National High Magnetic Field Laboratory, Tallahassee, Florida 32310, USA*

[5]*San Jose Research Center, Hitachi Global Storage Technologies, San Jose, California 95120, USA*

[6]*Department of Physics and Astronomy and HPC² Center for Computational Sciences, Mississippi State University, Mississippi State, Mississippi 39762, USA*

(Dated: February 1, 2008)

Abstract

The two-dimensional kinetic Ising model, when exposed to an oscillating applied magnetic field, has been shown to exhibit a nonequilibrium, second-order dynamic phase transition (DPT), whose order parameter Q is the period-averaged magnetization. It has been established that this DPT falls in the same universality class as the equilibrium phase transition in the two-dimensional Ising model in zero applied field. Here we study for the first time the scaling of the dynamic order parameter with respect to a nonzero, period-averaged, magnetic 'bias' field, H_b, for a DPT produced by a square-wave applied field. We find evidence that the scaling exponent, δ_{d}, of H_b at the critical period of the DPT is equal to the exponent for the critical isotherm, δ_{e}, in the equilibrium Ising model. This implies that H_b is a significant component of the field conjugate to Q. A finite-size scaling analysis of the dynamic order parameter above the critical period provides further support for this result. We also demonstrate numerically that, for a range of periods and values of H_b in the critical region, a fluctuation-dissipation relation (FDR), with an effective temperature $T_{\mathrm{eff}}(T, P, H_0)$ depending on the period, and possibly the temperature and field amplitude, holds for the variables Q and H_b. This FDR justifies the use of the scaled variance of Q as a proxy for the nonequilibrium susceptibility, $\partial \langle Q \rangle / \partial H_b$, in the critical region.

PACS numbers: 05.70.Ln, 64.60.Ht, 89.75.Da, 75.70.Cn

---

*Corresponding author: drobb@clarkson.edu

I. INTRODUCTION

The dynamic phase transition (DPT) in a ferromagnetic system below its critical temperature was first observed in numerical solutions of a mean-field model exposed to an oscillating magnetic field [1, 2]. It was then studied further, both in mean-field models [3, 4, 5, 6] and in kinetic Monte Carlo (KMC) simulations [5, 6, 7, 8, 9, 10]. A review of this early work can be found in Ref. [11]. More recently, the study of the DPT has expanded to include varying (and often more physical) model geometries. These include mean-field studies of domain-wall motion in an anisotropic XY model in one dimension [12, 13, 14], KMC simulations of a three-dimensional Ising system [15], and KMC simulations of a uniaxially anisotropic Heisenberg system in an off-axial field [16], an elliptically polarized applied field [17], and with the effect of a thin-film surface energy [18, 19, 20]. The phenomenon has also been observed in simulations of CO oxidation under oscillating CO pressure [21, 22]. Further simulation studies of the DPT in the two-dimensional kinetic Ising model have appeared [23, 24, 25, 26, 27], as well as analytical studies of the DPT [28, 29, 30, 31].

Here, we concentrate on the DPT in the two-dimensional kinetic Ising model. It was observed in simulations of this model that there exists a singularity at a critical period of the applied oscillating field [9, 10], and that the critical exponents β and γ (and, with less accuracy, ν) are consistent with the universality class of the equilibrium two-dimensional Ising transition in zero field [23] ($\beta = 1/8, \gamma = 7/4,$ and $\nu = 1$). In those studies, the techniques of finite-size scaling were extended to the study of the dynamic order parameter (Q, defined in Sec. II) in the non-equilibrium steady state. This provided evidence for a diverging correlation length at a critical value of the period. In particular, because the field conjugate to Q and a fluctuation-dissipation relation were not known, a susceptibility could not be measured directly, and the scaled variance $X_L^Q = L^2 \left(\langle Q^2 \rangle - \langle Q \rangle^2 \right)$, where L is the linear system size, was used as a proxy. An analytical argument, based on the correspondence of the two-dimensional kinetic Ising model and the continuous, two-dimensional Ginzburg-Landau model at the equilibrium critical point, provided an effective Hamiltonian for the non-equilibrium system and confirmed that the DPT is in the Ising universality class [28]. These findings are consistent with earlier symmetry arguments that any continous phase transition in a stochastic cellular automaton that preserves the Ising up-down symmetry should be in the equilibrium Ising universality class [32, 33].

Recently, experiments were performed on a $[\mathrm{Co}(0.4\mathrm{nm})/\mathrm{Pt}(0.7\mathrm{nm})]_3$ multilayer film with strong uniaxial anisotropy [34], whose equilibrium behavior is known to be Ising-like [35, 36]. The film was exposed to an oscillating (sawtooth) applied field with varying period, in the presence of constant 'bias' magnetic fields H_b of varying strength and sign. (The bias field is defined explicitly in Sec. II.) The behaviors of the dynamic order parameter and its variance, as functions of the applied field period and the bias field, provided strong evidence for the presence of the DPT in this experimental system. The observed behavior of the order parameter with respect to the bias field supported previous conjectures that the conjugate field could include the period-averaged magnetic field as an important component, and stimulated the numerical investigations in this paper.

This paper is organized as follows. In Sec. II, we describe the two-dimensional kinetic Ising model and our computational methods. In Sec. III, we verify directly the scaling of the dynamic order parameter with respect to the period-averaged magnetic field at the critical period, with scaling exponent $\delta_\mathrm{d} \approx \delta_\mathrm{e} = 15$, in agreement with the equilibrium Ising transition. In Secs. IV and V, we derive the expected asymptotic scaling functions in a finite-size scaling analysis of the dynamic phase transition with non-zero period-averaged bias field, and then compare the expected scaling of the dynamic order parameter to our numerical results. In Sec. VI, we present numerical data assessing the applicability of a fluctuation-dissipation relation (FDR) to this far-from-equilibrium system. We then in Sec. VII compare the expected scaling of the susceptibility (of the dynamic order parameter) to our numerical data, using the results of Sec. VI to reconcile our findings with previous results on the scaling of the fluctuations of the dynamic order parameter. Finally, we present a summary of our results in Sec. VIII.

II. COMPUTATIONAL MODEL

In order to facilitate comparison with previous results, we employ the same model and computational method as in Ref. [23]. Specifically, we perform kinetic Monte Carlo (KMC) simulations of a two-dimensional periodic square lattice of Ising spins S_i, which can take only the values $S_i = \pm 1$. The Hamiltonian of the model is

$$\mathcal{H} = -J \sum_{\langle i,j \rangle} S_i S_j - H(t) \sum_i S_i, \tag{1}$$

where $J > 0$ is the ferromagnetic exchange interaction, $\sum_{\langle i,j \rangle}$ runs over all nearest-neighbor pairs, $\sum_i$ runs over all L^2 lattice sites, and $H(t)$ is an oscillating, spatially uniform applied magnetic field. The form of $H(t)$ is here taken as a square wave with amplitude $H_0 = 0.3J$ and period P, measured in Monte Carlo steps per spin (MCSS). The square-wave form not only allows for more efficient KMC simulation, but also reduces the critical period and the finite-size effects for the DPT [23]. Other symmetric field shapes, such as sinusoidal [9, 10] and sawtooth [34], yield essentially the same results, but with a larger critical period and with stronger finite-size effects. The Glauber single-spin-flip MC algorithm with updates at randomly chosen sites is used, in which each attempted spin flip is accepted with probability

$$W\left(S_i \rightarrow -S_i\right) = \frac{1}{1 + \exp\left(\Delta E / T\right)}, \tag{2}$$

where ΔE is the energy change that would result from acceptance of the spin flip, and T is the absolute temperature in energy units (i.e., with Boltzmann's constant set to unity). All simulations were performed at $T = 0.8T_c$, where $T_c = 2.269J$ is the equilibrium critical temperature of the square-lattice Ising ferromagnet in zero applied field [37].

The system responds to the oscillating field via the time-dependent magnetization per site,

$$m(t) = \frac{1}{L^2} \sum_{i=1}^{L^2} S_i(t). \tag{3}$$

The dynamic order parameter is defined as the average of $m(t)$ over a given field cycle i [1] :

$$Q_i = \frac{1}{P} \int_{(i-1)P}^{iP} m(t) dt. \tag{4}$$

We define the bias field, so named because it measures the shift (or 'bias') of the periodic field toward either negative or positive field values, as the period-averaged magnetic field,

$$H_b = \frac{1}{P} \int_0^P H(t) dt. \tag{5}$$

This definition applies generally to any periodic magnetic field $H(t)$. In this paper, the applied field consists of a square wave with period P superposed with a constant magnetic field. Applying (5), since the period-average of the square-wave field is zero, the bias field H_b in this case is simply equal to the superposed constant magnetic field.

III. SCALING WITH RESPECT TO THE BIAS FIELD

In the two-dimensional equilibrium Ising model, the critical isotherm is given (in the thermodynamic limit, i.e., as $L \to \infty$) as

$$m\left(T = T_c, H \to 0\right) \propto H^{1/\delta_{\mathrm{e}}}, \tag{6}$$

where the critical exponent $\delta_{\mathrm{e}} = 15$ [38]. For finite systems, this relationship breaks down when the infinite-system correlation length, $\xi_\infty\left(T = T_c, H\right)$, which diverges as $H \to 0$, becomes comparable to the linear system size L. The relationship also naturally breaks down at larger fields away from the critical region. Therefore, a plot of m vs H for a given system size L will follow the power law (6) for a range of H near the critical value $H = 0$, with this range extending to smaller H as L is increased [39].

We can determine directly whether the non-equilibrium system exhibits a similar relationship,

$$\langle Q \rangle \left(P = P_c, H_b \to 0\right) \propto H_b^{1/\delta_{\mathrm{d}}} \tag{7}$$

in an analogous way. In Fig. 1, we plot $\langle Q \rangle$ vs H_b at the critical value of the period, $P = P_c$. In previous work, the reversal time for the magnetization, following instantaneous reversal of the uniform magnetic field H at $(H = 0.3J, T = 0.8T_c)$, was found as $\tau = 74.5977$ MCSS [9, 10]. The critical scaled half-period for the square waveform was determined to be $\Theta_c = P_c/\left(2\tau\right) = 0.918 \pm 0.005$ [23]. This yields $P_c = 136.96 \pm 0.75$ MCSS, and in our simulations and analysis in this paper we use $P_c = 136.96$ MCSS.

A power-law dependence is indeed seen to hold in Fig. 1, within a range which extends to lower values of H_b as L is increased. We fit the $L = 256$ data between the points labeled A and B in Fig. 1, finding a statistically significant fit with power-law exponent $\delta_{\mathrm{d}} = 14.85 \pm 0.18$. As including points with $H_b \geq 0.01J$ was found to greatly reduce the statistical significance of the fit, the value $H_b = 0.01J$ serves as a boundary of the scaling region at $P = P_c$. This result is consistent with an exponent $\delta_{\mathrm{d}} = \delta_{\mathrm{e}} = 15$, suggesting that the bias field H_b, for these parameters and the square waveform, is the dominant component of a conjugate field which exhibits the same scaling exponent in the DPT as does the applied magnetic field in the equilibrium Ising transition.

IV. FINITE-SIZE SCALING ANALYSIS WITH BIAS FIELD

To provide more complete evidence that H_b is the dominant component of the field conjugate to $\langle Q \rangle$, in the next several sections we will demonstrate data collapse onto a two-parameter finite-size scaling function for the system-size dependent quantity $\langle Q \rangle_L$ at points $(P \geq P_c, H_b > 0)$, for lattice sizes $L = 90, 128, 180$, and (in several cases) $L = 256$, using the critical exponents for the equilibrium Ising system. In this section, we briefly review the theory of finite-size scaling as it applies to this system. We then determine the expected asymptotic forms of the scaling functions, which are compared in later sections of the paper to our computational data.

The theory of finite-size scaling [40, 41] states that near a continuous phase transition, the singular part of the free-energy density for a d-dimensional system of linear size L can be written as

$$f_L \approx L^{-d} Y_\pm \left(|\epsilon| L^{1/\nu}, H L^{\beta\delta/\nu} \right), \tag{8}$$

where $\epsilon = (T - T_c)/T_c$, H (in units of $k_B T$) is the field conjugate to the order parameter, ν is the critical exponent for the correlation length, β is the exponent for the order parameter, δ is the exponent for the critical isotherm, and $Y_\pm$ are scaling functions above ($+$) and below ($-$) the critical point. This yields for the order parameter at finite L

$$m_L = \frac{\partial f}{\partial H} = L^{-\beta/\nu} \mathcal{F}_{0\pm} \left(|\epsilon| L^{1/\nu}, H L^{\beta\delta/\nu} \right), \tag{9}$$

where the exponent for L in the prefactor is obtained by using the hyperscaling relation $d\nu = 2 - \alpha$ and the exponent equality $\alpha = 2 - \beta(\delta + 1)$. Further differentiation yields the susceptibility,

$$\chi_L = \frac{\partial m_L}{\partial H} = L^{\gamma/\nu} \mathcal{G}_{0\pm} \left(|\epsilon| L^{1/\nu}, H L^{\beta\delta/\nu} \right), \tag{10}$$

where the exponent for L in the prefactor is obtained by using the exponent equality $\gamma = \beta(\delta - 1)$.

It has previously been shown analytically that the DPT for a sinusoidal applied field, which is symmetric under $H(t) \to -H(t + P/2)$ and so which can safely be assumed to have $H_c = 0$, has an effective Ginzburg-Landau free-energy density in the same universality class as the equilibrium Ising model [28]. It therefore appears reasonable to write corresponding scaling functions for the dynamic order parameter $\langle Q \rangle$ and its associated susceptibility $\hat{\chi}$,

$$\langle Q \rangle_L = L^{-\beta/\nu} \mathcal{F}_\pm \left(|\theta| L^{1/\nu}, (H_c/J) L^{\beta\delta/\nu} \right), \tag{11}$$

7

and

$$\hat{\chi}_L = L^{\gamma/\nu} \mathcal{G}_\pm \left(|\theta| L^{1/\nu}, (H_c/J) L^{\beta\delta/\nu} \right) , \qquad (12)$$

where $\theta = (P - P_c)/P_c$, and H_c is the (as yet unknown) field conjugate to $\langle Q \rangle$. In this paper we express H_c (and H_b) in units of the exchange constant, J, so that the second scaling parameter in Eqs. 11 and 12 is dimensionless. The specific form, H_c/J, with which H_c is assumed to enter the second scaling parameter needs more theoretical investigation, and could conceivably change as the theory of the DPT is further developed. However, this should not affect our conclusions [42]. Computational results for sinusoidal and square-wave fields, which both are symmetric under $H(t) \to -H(t+P/2)$ and so presumably have $H_c = 0$, have previously confirmed the scaling behavior with respect to θ. The exponent values were determined as $\gamma/\nu = 1.74 \pm 0.05$, $\beta/\nu = 0.126 \pm 0.005$, and $\nu = 0.95 \pm 0.15$ [23], consistent with the exact values for the two-dimensional equilibrium Ising model, $\gamma = 7/4 = 1.75$, $\beta = 1/8 = 0.125$, and $\nu = 1$.

We now determine the expected asymptotic forms of the scaling functions $\mathcal{F}_+(y_1, y_2)$ and $\mathcal{G}_+(y_1, y_2)$, where we emphasize that the $+$ subscript indicates that the scaling functions refer to the range $P \geq P_c$, and where the scaling parameters are $y_1 \equiv \theta L^{1/\nu}$ and $y_2 \equiv (H_c/J) L^{\beta\delta/\nu}$.

$\underline{y_1 \gg y_2}$. We expect $\hat{\chi}_L \sim \theta^{-\gamma} = L^{\gamma/\nu} y_1^{-\gamma}$ (independent of y_2) and $\langle Q \rangle_L = \hat{\chi}_L H_c \sim \theta^{-\gamma} H_c \sim L^{-\beta/\nu} y_1^{-\gamma} y_2$, where $\gamma = \beta(\delta - 1)$ was used to obtain the exponent for L in $\langle Q \rangle_L$.

$\underline{y_1 \ll y_2}$. We expect that $\langle Q \rangle_L \sim H_c^{1/\delta} \sim L^{-\beta/\nu} y_2^{1/\delta}$ and $\hat{\chi}_L = \partial \langle Q \rangle_L / \partial H_c \sim L^{\gamma/\nu} y_2^{(1-\delta)/\delta}$ (both independent of y_1), where $\gamma = \beta(\delta - 1)$ was used to obtain the exponent for L in $\hat{\chi}_L$. Thus, the asymptotic forms of the scaling functions are expected to be

$$\mathcal{F}_+(y_1, y_2) \equiv L^{\beta/\nu} \langle Q \rangle_L \sim \begin{cases} y_1^{-\gamma} y_2 & \text{for } y_1 \gg y_2 \\ y_2^{1/\delta} & \text{for } y_1 \ll y_2 \end{cases} \qquad (13)$$

and

$$\mathcal{G}_+(y_1, y_2) \equiv L^{-\gamma/\nu} \hat{\chi}_L \sim \begin{cases} y_1^{-\gamma} & \text{for } y_1 \gg y_2 \\ y_2^{(1-\delta)/\delta} & \text{for } y_1 \ll y_2 \end{cases} . \qquad (14)$$

V. COMPARISON OF FIRST SCALING FUNCTION TO COMPUTATIONAL RESULTS

In Fig. 2(a), using the equilibrium values β_e and ν_e in calculating $\mathcal{F}_+(y_1, y_2) \equiv L^{\beta/\nu} \langle Q \rangle_L$, we present a plot of the scaling function $\mathcal{F}_+$ vs y_1 for different values of y_2, for lattice

sizes $L = 90$, 128, and 180. Here and for the remainder of the paper, exponents with the subscripts 'd' and 'e' refer to the behavior of the nonequilibrium system (with a dynamic phase transition) and the equilibrium system, respectively. The scaling function exhibits a power-law dependence in the regime $y_1 \gg y_2$, which is consistent with Eq. (13). At progressively larger values of the constant y_2, the power-law scaling can be seen to begin at increasing values of y_1, as would be expected. A best-fit line to the final five points of the $L = 180$ data at $y_2 = 3.39$ yields an estimate of the scaling exponent $-\gamma_{\rm d} = -1.76 \pm 0.07$ in Eq. (13). This is consistent with the previous results for $H_c = 0$ cited above [23], and it supports the hypothesis that $\gamma_{\rm d} = \gamma_{\rm e} = 7/4 = 1.75$. In Fig. 2(b), we present just the data for $y_2 = 3.39$, including additional data points at $y_1 = 280$ and 477. The data deviate from the power-law behavior for $L = 90$ at $y_1 > 149$, for $L = 128$ at $y_1 > 280$, and for $L = 180$ at $y_1 > 477$. This locates the boundary of the scaling regime (for $y_2 = 3.39$) at $\theta = y_1/L^{1/\nu} \approx 2.65$.

In Fig. 3, again using $\beta_{\rm e}$ and $\nu_{\rm e}$ in calculating $\mathcal{F}_+$, we plot the scaling function $\mathcal{F}_+$ vs y_2 at different values of y_1, in order to examine the scaling behavior for $y_1 \gg y_2$. For the constant values $y_1 = 43.4, 69.7$, and 149, power-law scaling can be observed in the regime $y_1 \gg y_2$. A best-fit line to the $y_1 = 149$ data for the five points from $y_2 = 3.39$ to 84.6 yields a scaling exponent of 1.01 ± 0.01, which is consistent with the value of 1 expected from Eq. (13).

In order to investigate the scaling of $\mathcal{F}_+$ in the asymptotic limit $y_1 \ll y_2$, we plot in Fig. 4 the scaling function $\mathcal{F}_+(y_1, y_2)$ vs y_2 at the critical period $P = P_c$ (i.e., $y_1 = 0$), at lattice sizes $L = 128, 180$, and 256. In the range $20 < y_2 < 50$, power-law scaling is observed for all three lattice sizes. For $y_2 > 50$, the data deviate from power-law scaling, with the smallest lattice size deviating first, as expected in a finite-size scaling plot. A fit of the $L = 256$ data in the range from $y_2 = 8.46$ to 84.6 produces a scaling exponent 0.0673 ± 0.0008. Since the constant factors $L^{\beta\delta/\nu}$ and $L^{\beta/\nu}$ do not affect the fit of the scaling exponent, this is the same exponent found in the fit of $\langle Q \rangle$ vs H_b in Fig. 1. The reciprocal of this scaling exponent is thus $\delta_{\rm d} = 14.85 \pm 0.18$, which is consistent with the exponent of the critical isotherm, $\delta_{\rm e} = 15$, in the equilibrium Ising model.

The comparison of the second scaling function, $\mathcal{G}_+(y_1, y_2)$, to numerical data is more clearly presented after the relationship of the susceptibility $\hat{\chi}_L$ and the scaled variance X_L^Q has been examined. Therefore, we present in the next section numerical results on the extent

9

of applicability of an FDR between $\hat{\chi}_L$ and X_L^Q, before turning in Sec. VII to the second scaling function.

VI. APPLICABILITY OF A FLUCTUATION-DISSIPATION RELATION

FDRs, such as the Einstein relation, Green-Kubo relations, etc., hold a central place in equilibrium statistical mechanics. This is essentially a consequence of detailed balance and the role of the partition function as a moment-generating function, and thus such relations cannot be readily extended to nonequilibrium steady states. However, it has recently been shown that certain FDRs can be extended to far-from equilibrium steady states by use of an *effective temperature* [43, 44]. Here we will therefore consider whether the nonequilibrium susceptibility and the scaled variance of the dynamic order parameter can be related as

$$\hat{\chi}_L \equiv \frac{\partial \langle Q \rangle_L}{\partial H_b} = \frac{L^2 \left(\langle Q^2 \rangle_L - \langle Q \rangle_L^2 \right)}{T_{\text{eff}}} \equiv \frac{X_L^Q}{T_{\text{eff}}}, \tag{15}$$

with an effective temperature T_{eff}, in a way analogous to the equilibrium FDR,

$$\chi_L \equiv \frac{\partial \langle m \rangle_L}{\partial H} = \frac{L^2 \left(\langle m^2 \rangle_L - \langle m \rangle_L^2 \right)}{T}, \tag{16}$$

in which T is the temperature. As mentioned in Secs. I and IV, this conjecture motivated the use in previous work of the scaled variance X_L^Q as a proxy for $\hat{\chi}_L$ in investigating the scaling behavior of the nonequilibrium system near its critical period.

To test the extent to which Eq. (15) holds, we computed values of $\hat{\chi}_L$ and X_L^Q for a range of periods from $P = 140$ to 250 MCSS and a range of bias fields from $H_b = 0$ to an upper limit between $0.005J$ and $0.2J$. (The bias field necessary to 'saturate' the nonequilibrium system, i.e., to produce values of $\hat{\chi}_L$ and X_L^Q near zero, increases as the period is increased.) The computations were perfomed at $L = 180$. The quantity $\hat{\chi}_L$ was computed directly as a numerical derivative:

$$\hat{\chi}_L(P, H_b) \approx \left(\langle Q \rangle(P, H_b + \Delta H_b) - \langle Q \rangle(P, H_b - \Delta H_b) \right) / 2\Delta H_b. \tag{17}$$

The choice of $\Delta H_b = 0.1 H_b$ was found to produce sufficiently accurate values of the numerical derivative across the range of bias fields studied. The results for periods $P = 140$ through 190 MCSS are shown in Fig. 5. A linear relationship is seen to exist between $\hat{\chi}_L$ and X_L^Q, for each value of P, over a wide range of $\hat{\chi}_L$ values. At each period, the dependence becomes

10

nonlinear below a certain value of $\hat{\chi}_L$, as illustrated for periods $P = 150$, 170, and 190 MCSS in Fig. 6. Since low values of the susceptibility $\hat{\chi}_L$ correspond to large values of the bias field H_b, we interpret this breakdown of linearity as an indication that the FDR in Eq. (15) holds only in a scaling regime around the critical point, i.e., for a limited range of H_b around $H_b = 0$.

The relationship between X_L^Q and $\hat{\chi}_L$ at the higher periods, $P = 220$ and $P = 250$ MCSS, is more complicated, as shown in Fig. 7. At $P = 220$ MCSS, following the nonlinear regime at low $\hat{\chi}_L$, there is a linear relationship with slope $T_{\text{eff}} = (6.27 \pm 0.11)J$ up to $\hat{\chi}_L \approx 13\ J^{-1}$, followed by a second distinct linear dependence with slope $T_{\text{eff}} \approx (4.16 \pm 0.29)J$ above $\hat{\chi}_L = 13\ J^{-1}$. At $P = 250$ MCSS, the initial nonlinear dependence is again present. Then the first linear regime has $T_{\text{eff}} = (6.49 \pm 0.07)J$ up to $\hat{\chi}_L \approx 13\ J^{-1}$, and is followed by a regime which can be characterized as either linear with very gentle slope $(0.27 \pm 0.22)J$, or as an effective 'saturation' of X_L^Q past $\hat{\chi}_L = 13\ J^{-1}$.

In Fig. 8 we plot the best-fit slopes from Figs. 5 and 7, which according to Eq. (15) represent estimates of T_{eff}, vs the scaling parameter $\theta = (P - P_c)/P_c$. We have included in the plot the slopes of both linear regimes for the values $\theta = 0.606$ and 0.825 ($P = 220$ and 250 MCSS). For θ below 0.4 ($P \approx 190$ MCSS), T_{eff} increases with θ in a way not inconsistent with a linear relationship (with slope $2.97J$). It may be interesting to note that an extrapolation of the linear relationship to $\theta = 0$ ($P = P_c$) yields the value $T_{\text{eff}} = 3.39J$, which is significantly higher than the critical temperature, $T_c = 2.2619J$, of the equilibrium Ising system. However, one should not put too much emphasis on the numerical values of T_{eff} [45], as they could easily be changed. For instance, if H_b is only *proportional to* the full conjugate field H_c, with a proportionality constant different from unity, this would trivially change T_{eff} in Eq. (15). The important result, which we have demonstrated to hold in the critical region, is the linear relationship between X_L^Q and $\hat{\chi}_L$.

We can thus characterize the extent of applicability of an FDR to the DPT above the critical period as follows. For $\theta < 0.4$, an FDR holds outside of a small nonlinear regime at low $\hat{\chi}_L$ (high H_b), with an effective temperature T_{eff} which increases approximately linearly with θ. For θ above 0.4, two linear relationships appear to exist between X_L^Q and $\hat{\chi}_L$ in separate regimes, making it impossible to define a unique T_{eff} at a given value of θ. An understanding of the nonlinear regime, which is present at low $\hat{\chi}_L$ for all periods examined, as well as of the complication of the FDR above $\theta = 0.4$, would be highly desirable. We hope

that these numerical results can stimulate the development of, as well as test the accuracy of, a theoretical description of the non-equilibrium steady states produced in the presence of non-zero H_b for this DPT.

VII. COMPARISON OF SECOND SCALING FUNCTION TO COMPUTATIONAL RESULTS

We now test the asymptotic scaling forms for $\mathcal{G}_+$ in Eq. (14). First, we note that in performing least-squares fits, one normally requires the goodness-of-fit parameter q, i.e., the probability that (assuming the fit relationship were true) random error alone could produce the observed data, to be greater than 10^{-3} to consider the fit reasonable. Within this section, however, and in the captions to Figs. 9 through 11, it will be useful for descriptive purposes to refer to scaling exponents resulting from attempts at least-squares fits with q values below this acceptable range. We will refer to the results of such unsuccessful fitting attempts as 'nominal' scaling exponents, and for clarity will report the value of the parameter q for each scaling exponent presented in this section.

In Fig. 9, we plot the scaling function $\mathcal{G}_+$ vs y_1 for $y_2 = 8.46$ at $L = 180$, using γ_e and ν_e to calculate $\mathcal{G}_+$, and evaluating $\hat{\chi}_L$ numerically according to Eq. (17). In addition, we plot in the same figure the scaling function $\mathcal{G}_+^X(y_1, y_2) \equiv X_L^Q L^{-\gamma/\nu}$ vs y_1, for the same values of y_2 and L. A fit to all four $\mathcal{G}_+$ data points yields a scaling exponent -1.60 ± 0.03 ($q = 0.02$), while a fit to the last three $\mathcal{G}_+$ data points yields a scaling exponent -1.71 ± 0.05 ($q = 0.25$). We will provide evidence in the next paragraph that only the last three $\mathcal{G}_+$ data points, and not the first, satisfy the asymptotic condition $y_1 \gg y_2$. Thus, these data are consistent with power-law scaling of $\hat{\chi}_L$ with exponent $-\gamma_d = -\gamma_e = -7/4 = -1.75$. Attempts to fit the $\mathcal{G}_+^X$ data to all four and the last three data points yield nominal scaling exponents -1.73 ± 0.01 ($q < 10^{-15}$) and -1.81 ± 0.02 ($q = 2.3 \times 10^{-14}$), respectively. Thus, while in Fig. 9 it appears that the power-law relationships with these nominal scaling exponents give respectable visual fits to the $\mathcal{G}_+^X$ data, there are variations in the data which, while small, are larger than the statistical error bars, and which prevent a statistically significant fit. We will describe the causes of these variations later in this section.

We present in Fig. 10 a plot of $\mathcal{G}_+$ and $\mathcal{G}_+^X$ vs y_1 at $y_2 = 0$, again for $L = 180$, for a larger range from $y_1 = 30.3$ to 477. With $y_2 = 0$, we expect that $y_1 = 30.3$ (and indeed,

essentially any nonzero value of y_1) should satisfy the asymptotic scaling condition $y_1 \gg y_2$. An attempt to fit to all six $\mathcal{G}_+$ data points in Fig. 10 gives a nominal scaling exponent -1.65 ± 0.03 ($q = 3.8 \times 10^{-7}$), while a fit to the first five points ($y_1 = 30.3$ through 280) gives a scaling exponent -1.74 ± 0.03 ($q = 0.07$). Excluding the first data point at $y_1 = 30.3$ has little effect on either fit. This supports the assumption that with $y_2 = 0$, the asymptotic scaling condition $y_1 \gg y_2$ holds for $y_1 = 30.3$, while for $y_2 = 8.46$, as used in Fig. 9, the asymptotic scaling condition does not hold for $y_1 = 30.3$. Attempts to fit all of, and the first five of, the $\mathcal{G}_+^X$ data points to power-law scaling again yield only nominal scaling exponents -2.01 ± 0.01 ($q < 10^{-15}$) and -2.10 ± 0.01 ($q < 10^{-15}$), respectively.

We considered that the low statistical significance of the fits to the $\mathcal{G}_+^X$ data could be caused by underestimation of the error bars on X_L^Q. These error bars were calculated by (i) finding the correlation time in the numerical data series Q_i from the simulation, and sampling data at intervals of twice the correlation time; (ii) dividing this sampled data into $k > 16$ groups and calculating the value of X_L^Q within each group; (iii) finding the mean and standard error of this collection of X_L^Q values. As a check on self-consistency, we performed several independent calculations of X_L^Q by this method, and found that the standard error of these values (corrected for small sample size) was comparable to the standard error found within each calculation. Thus, we have strong evidence that the error bars for X_L^Q (and $\mathcal{G}_+^X$) are accurate.

These scaling results can be understood in light of the observations in Sec. VI on the relationship between X_L^Q and $\hat{\chi}_L$. We can reasonably assume that the breakdown in scaling of $\mathcal{G}_+$ past $y_1 = 280$ ($P = 350$ MCSS, $\theta = 1.56$) in Fig. 10 occurs because this is the boundary of the critical region. The small variations of the $\mathcal{G}_+^X$ data for $P < 350$ MCSS in Fig. 10 from a scaling relationship with exponent $-\delta_{\rm d} = -1.75$ then have three main causes. The first cause is the multiplication of the accurately scaling function $\mathcal{G}_+$ by the θ- and y_1-dependent value $T_{\rm eff}$, according to Eq. (15). However, such a variation would also occur in an analogous plot for the scaling of $X_L^M \equiv L^2 (\langle m^2 \rangle - \langle m \rangle^2)$ vs $y_{1,\rm e} = \epsilon L^{1/\nu} = ((T - T_c)/T_c) L^{1/\nu}$ in the equilibrium Ising model, since the susceptibility $\chi_L^M \equiv \partial \langle m \rangle / \partial H$ scales with exponent $-\gamma_{\rm e}$, and X_L^M is related to χ_L^M by the ϵ-dependent temperature T according to Eq. (16). This effect is small enough to be neglected in equilibrium critical scaling, and, since the change in $T_{\rm eff}$ from $\theta = 0.02$ to $\theta = 0.4$ is comparable to the change in T from $\epsilon = 0.02$ to $\epsilon = 0.4$ in the equilibrium transition, it can also be neglected here. The second cause is the presence of the

nonlinear regimes in the plots of X_L^Q vs $\hat{\chi}_L$ at low $\hat{\chi}_L$, resulting in non-zero X_L^Q-intercepts in the application of Eq. (15) to Figs. 5 and 7. Because of this, division of the X_L^Q data by the appropriate T_{eff} values (given in the caption of Fig. 5) does not quite reproduce the corresponding $\hat{\chi}_L$ data, and (even below $\theta = 0.4$) does not quite result in scaling consistent with $\delta_{\text{d}} = 1.75$ with statistical signficance. The third and most signficant cause of the variations of the $\mathcal{G}_+^X$ data is the 'doubly linear' behavior observed in Fig. 7 for $\theta > 0.4$, which prevents identification of a unique T_{eff} in this range.

The assumption that X_L^Q can be used as a proxy for $\hat{\chi}_L$ is thus fairly well justified close to the critical period, where T_{eff} varies over a limited range and the more complicated effects observed at $\theta > 0.4$ are not relevant. This is supported by Fig. 9, where the data points cluster closely around the line corresponding to power-law scaling with exponent $-1.73 \approx -\gamma_{\text{e}}$. However, because of the first two causes just described, there are small systematic variations in the $\mathcal{G}_+^X$ data which prevent a statistically significant fit to a pure power-law relationship as a function of y_1.

In order to clarify the relationship of these scaling results to those in previous work, we also plot in Fig. 11 data of $\mathcal{G}_+^{|X|}(y_1, y_2) \equiv X_L^{|Q|} L^{-\gamma/\nu} \equiv \left(\langle Q^2 \rangle - \langle |Q| \rangle^2 \right) L^{-\gamma/\nu}$ vs y_1 at $y_2 = 0$, again using the equilibrium values γ_{e} and ν_{e} to calculate $\mathcal{G}_+^{|X|}$. This can be directly compared to Fig. 11(d) in Ref. [23], in which the quantity we call $X_L^{|Q|}$ was called X_L^Q. Attempted fits to all five data points and to the last four data points of $\mathcal{G}_+^{|X|}$ in Fig. 10 produce nominal scaling exponents -1.60 ± 0.02 and -1.69 ± 0.02 (both with $q < 10^{-15}$). The agreement in Fig. 11(d) of Ref. [23] of the line with slope $-7/4$ with the data for $\theta > \theta_c$ must therefore be viewed as qualitative. The method used in Ref. [23] to numerically estimate γ_{d}, however, which involves finite-size scaling at the critical period, is fully consistent with the results of this paper, since at each period with $\theta < 0.4$ we have found that the FDR in Eq. (15) holds to a very good approximation.

Finally, in Fig. 12, we plot $\mathcal{G}_+^X$ vs y_2 at $P = P_c$, to study its scaling in the regime $y_1 \ll y_2$. As just noted, the use of X_L^Q as a proxy for $\hat{\chi}_L$ is well justified at $P = P_c$ by our results. Power-law scaling is perhaps suggested in the range $20 < y_2 < 50$ for $L = 180$, and it is clearly obeyed from $y_2 = 8.42$ to 84.2 for $L = 256$. The scaling exponent was determined as $(1 - \delta_{\text{d}})/\delta_{\text{d}} = -0.914 \pm 0.030$, which is consistent with the corresponding equilibrium value $(1 - \delta_{\text{e}})/\delta_{\text{e}} = -14/15 \approx -0.933$.

VIII.   CONCLUSIONS AND OUTLOOK

In this article, we have continued the computational study of the dynamic phase transition (DPT) in the two-dimensional kinetic Ising model exposed to a periodically oscillating field, which was begun in Refs. [9, 10, 23]. We have established two distinct but related results about the field conjugate to the dynamic order parameter. First, we have identified the period-averaged magnetic field, or 'bias field', H_b as an important component of the full conjugate field. This claim is supported by numerical evidence that the dynamic order parameter and its susceptibility follow critical scaling with respect to H_b. In particular, the scaling exponent δ_{d} of the conjugate field was determined for the first time, and found by finite-size scaling analysis of large-scale kinetic Monte Carlo simulations to be equal to the critical-isotherm exponent for the equilibrium Ising transition, $\delta_{\mathrm{e}} = 15$. Furthermore, in agreement with previous results [23], the dynamic scaling exponents γ_{d}, β_{d}, and ν_{d} were also found to equal their equilibrium Ising counterparts, $\gamma_{\mathrm{e}} = 7/8$, $\beta_{\mathrm{e}} = 1/8$, and $\nu_{\mathrm{d}} = 1$.

These results further strengthen previous numerical [9, 10, 23] and analytical [28, 32, 33] claims that the DPT in a periodically driven two-dimensional kinetic Ising model belongs to the universality class of the equilibrium two-dimensional Ising model. However, with respect to the direct applicability of the symmetry arguments of Refs. [32, 33], we caution the reader that what is claimed in the present paper (as well as in Ref. [28]) is only equivalence of the *phase transitions* in the driven kinetic Ising model and the equilibrium Ising model. *Outside* the critical region, it is neither clear how closely $P - P_c$ and H_b play the roles of $T - T_c$ and the ordinary magnetic field, respectively, nor how closely the dynamic order parameter, Q, corresponds to the average equilibrium magnetization. From our discussion of the FDR in Sec. VI, it appears likely that one or more of these relations break down outside the critical region. Much theoretical work remains to be done in this area.

The second main result of this article is that a fluctuation-dissipation relation (FDR), that is, a proportionality relation between the scaled fluctuations $X_L^Q \equiv L^2 \left(\langle Q^2 \rangle - \langle Q \rangle^2 \right)$ and the susceptibility $\hat{\chi}_L$ with a slope we have called T_{eff}, holds for a range of periods above P_c and for a range of bias fields around $H_b = 0$. We stress again that we have found the FDR of Eq. (15) to hold *only in the critical region* in this nonequilibrium system, in contrast to the equilibrium FDR of Eq. (16) which follows directly from the partition function, and which thus holds everywhere. We note that, for the parameters used in our computation at least,

15

the critical region in which the nonequilibrium FDR holds ($P < 190$ MCSS) is somewhat smaller than the critical region in which power-law scaling is obeyed ($P < 350$ MCSS). In previous work, when the conjugate field had not been identified, the scaled fluctuations X_L^Q were used as a proxy for the (then unknown) quantity $\hat{\chi}_L$. The evidence for the FDR presented here shows this assumption to be fully justified at the critical period (see Fig. 12), and to be a very good approximation – nearly as good as the use of the scaled fluctuations as a proxy for the susceptibility in the equilibrium Ising model – in the critical region where the FDR holds.

There are at least three further computational projects suggested by the progress reported here. The first is to investigate whether the field H_b functions as the conjugate field, with scaling exponents consistent with the equilibrium Ising transition for periods $P < P_c$, below the critical period. In the equilibrium system, the study of critical scaling in nonzero field for $T < T_c$ is complicated by the long time correlations and strong finite-size effects which accompany the bimodal distributions of magnetization below T_c. Similar effects would complicate the investigation of scaling with respect to H_b in the DPT for $P < P_c$, but the advanced techniques [46, 47] which make the equilibrium simulations tractable do not extend obviously to the nonequilibrium case. The second computational project suggested is to determine the nature of the full conjugate field H_c. The third project would be to study the FDR at different values of the temperature, T, and the amplitude, H_0, of the driving field. Finally, we remark that it would be very desirable to extend the current understanding of the theory of nonequilibrium steady states to include the conjugate field H_b, the FDR found in the critical region, and the scaling of H_b.

[1] T. Tomé and M. J. de Oliveira, Phys. Rev. A **41**, 4251 (1990).

[2] J. F. F. Mendes and E. J. S. Lage, J. Stat. Phys. **64**, 653 (1991).

[3] M. F. Zimmer, Phys. Rev. E **47**, 3950 (1993).

[4] M. Acharyya and B. K. Chakrabarti, Phys. Rev. B **52**, 6550 (1995).

[5] M. Acharyya, Phys. Rev. E **56**, 2407 (1997).

[6] M. Acharyya, Phys. Rev. E **58**, 179 (1998).

[7] W. S. Lo and R. A. Pelcovits, Phys. Rev. A **42**, 7471 (1990).

[8] M. Acharyya, Phys. Rev. E **56**, 1234 (1997).

[9] S. W. Sides, P. A. Rikvold, and M. A. Novotny, Phys. Rev. Lett. **81**, 834 (1998).

[10] S. W. Sides, P. A. Rikvold, and M. A. Novotny, Phys. Rev. E **59**, 2710 (1999).

[11] B. K. Chakrabarti and M. Acharyya, Rev. Mod. Phys. **71**, 847 (1999).

[12] T. Yasui, H. Tutu, M. Yamamoto, and H. Fujisaka, Phys. Rev. E **66**, 036123 (2002).

[13] N. Fujiwara, H. Tutu, and H. Fujisaka, Phys. Rev. E **70**, 066132 (2004).

[14] N. Fujiwara, H. Tutu, and H. Fujisaka, Prog. Theor. Phys. Suppl. **161**, 181 (2006).

[15] Y. Z. Shao, W. R. Zhong, and G. M. Lin, Acta Physica Sinica **53**, 3165 (2004).

[16] M. Acharyya, Int. J. Mod. Phys. C **14**, 49 (2003).

[17] M. Acharyya, Phys. Rev. E **69**, 027105 (2004).

[18] H. Jang and M. J. Grimson, Phys. Rev. E **63**, 066119 (2003).

[19] H. Jang, M. J. Grimson, and C. K. Hall, Phys. Rev. B **67**, 094411 (2003).

[20] H. Jang, M. J. Grimson, and C. K. Hall, Phys. Rev. E **68**, 046115 (2003).

[21] E. Machado, G. M. Buendía, P. A. Rikvold, and R. M. Ziff, Phys. Rev. E **71**, 016120 (2005).

[22] G. M. Buendía, E. Machado, and P. A. Rikvold, J. Mol. Struct.: THEOCHEM **769**, 189 (2006).

[23] G. Korniss, C. J. White, P. A. Rikvold, and M. A. Novotny, Phys. Rev. E **63**, 016120 (2001).

[24] G. Korniss, P. A. Rikvold, and M. A. Novotny, Phys. Rev. E **66**, 056127 (2002).

[25] A. Chatterjee and B. K. Chakrabarti, Phys. Rev. E **67**, 046113 (2003).

[26] A. Chatterjee and B. K. Chakrabarti, Phase Transitions **77**, 581 (2004).

[27] M. Acharyya, Phys. Rev. E **59**, 218 (1999).

[28] H. Fujisaka, H. Tutu, and P. A. Rikvold, Phys. Rev. E **63**, 036109 (2001); **63**, 059903(E) (2001).

[29] H. Tutu and N. Fujiwara, J. Phys. Soc. Jpn. **73**, 2680 (2004).

[30] E. Z. Meilikhov, JETP Letters **79**, 620 (2004).

[31] S. B. Dutta, Phys. Rev. E **69**, 066115 (2004).

[32] G. Grinstein, C. Jayaprakash, and Y. He, Phys. Rev. Lett. **55**, 2527 (1985).

[33] K. E. Bassler and B. Schmittmann, Phys. Rev. Lett. **73**, 3343 (1994).

[34] D. T. Robb, Y. H. Xu, O. Hellwig, J. McCord, A. Berger, M. A. Novotny, and P. A. Rikvold, *Evidence for a dynamic phase transition in [Co/Pt]$_3$ magnetic multilayers* (2007), to be submitted to Phys. Rev. B.

[35] M. Bander and D. L. Mills, Phys. Rev. B **38**, R12015 (1988).

[36] C. Back, C. Würsch, A. Vaterlaus, U. Ramsperger, U. Maier, and D. Pescia, Nature **378**, 597 (1995).

[37] L. Onsager, Phys. Rev. **65**, 117 (1944).

[38] D. P. Landau and K. Binder, *A Guide to Monte Carlo Simulations in Statistical Physics* (Cambridge University Press, Cambridge, UK, 2000).

[39] K. Binder and D. P. Landau, Phys. Rev. B **30**, 1477 (1984).

[40] V. Privman and M. E. Fisher, Phys. Rev. B **30**, 322 (1984).

[41] V. Privman, in V. Privman, ed., *Finite Size Scaling and Numerical Simulation of Statistical Systems* (World Scientific, Singapore, 1990), pp. 4–98.

[42] Until the theory of the DPT, e.g. in Ref. [28], is extended to include H_c, it is unclear in what form it should enter the dimensionless scaling parameter, i.e. as H_c/J, H_c/k_BT, or otherwise. Here we have chosen the form H_c/J. Since our numerical data is all taken at a single temperature, $T = 0.8T_c = 1.8152J$, a change in this form would at most multiply values of y_2 by a constant factor, and would not affect the scaling relations reported in this paper.

[43] K. Hayashi and S.-I. Sasa, Phys. Rev. E **69**, 066119 (2004).

[44] K. Hayashi and S.-I. Sasa, Phys. Rev. E **71**, 046143 (2005).

[45] To avoid misunderstandings, note that it is certainly possible to define other sensible effective temperatures for an Ising-like model, so that one should be clear about the definition being used in a given context. For example, the nonequilibrium FDR proposed in Refs. [48, 49]

connects *two-time* response and correlation functions, and applies to critical ageing in a two-parameter family of Ising-like models. This family includes many models without detailed balance (e.g., the noisy voter and majority models), and one model – the equilibrium Ising model with Glauber dynamics – with detailed balance. In contrast, our Eq. (15) concerns *single-time* response and correlations, and the kinetic Ising model driven by an oscillating field is not included in the two-parameter family of models considered in Refs. [48, 49].

[46] B. A. Berg and T. Neuhaus, Phys. Rev. Lett. **68**, 9 (1992).

[47] B. A. Berg and T. Neuhaus, Phys. Lett. B **267**, 249 (1991).

[48] C. Godrèche and J. M. Luck, J. Phys. A: Math. Gen. **33**, 9141 (2000).

[49] F. Sastre, I. Dornic, and H. Chaté, Phys. Rev. Lett. **91**, 267205 (2003).
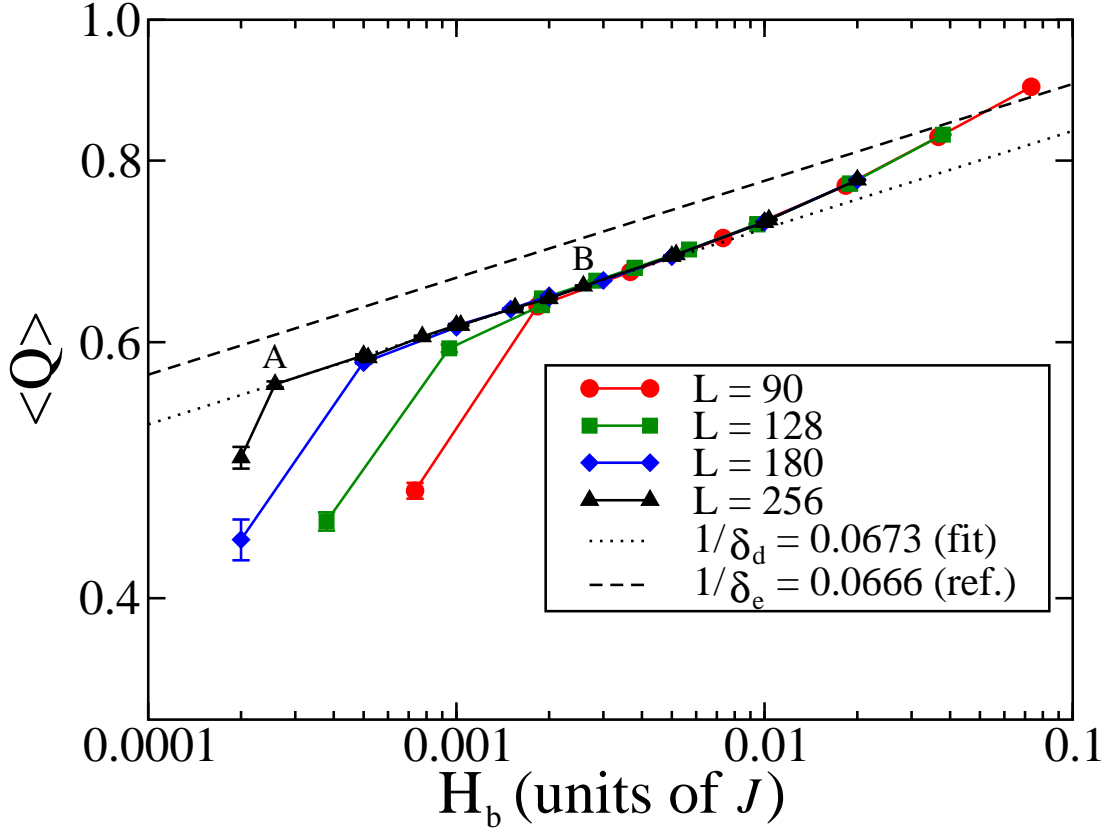
FIG. 1: (Color online.) Log-log plot of the dynamic order parameter, $\langle Q \rangle$, vs bias field, H_b, at $P = P_c$ for $L = 90, 128, 180,$ and 256. A least-squares fit to power-law scaling of the $L = 256$ data, in the range between the labels A and B above, produced a statistically significant fit with scaling exponent $1/\delta_d = 0.0673 \pm 0.0008$ (corresponding to $\delta_d = 14.85 \pm 0.18$). The dotted line corresponds to the scaling exponent $1/\delta_d = 0.0673$. A reference line representing scaling with the equilibrium Ising exponent, $\delta_e = 15$ ($1/\delta_e = 0.0666$), is shown as the dashed line.
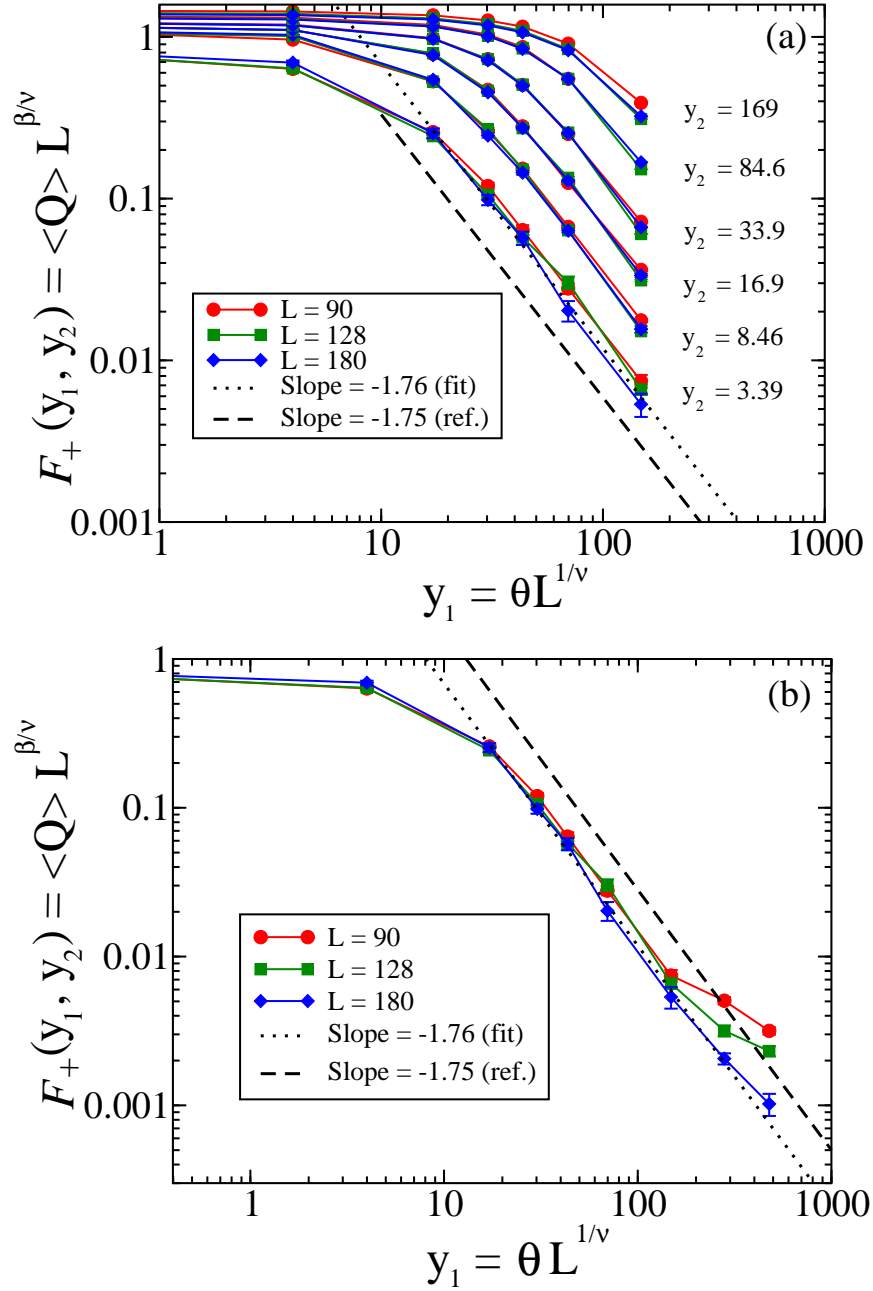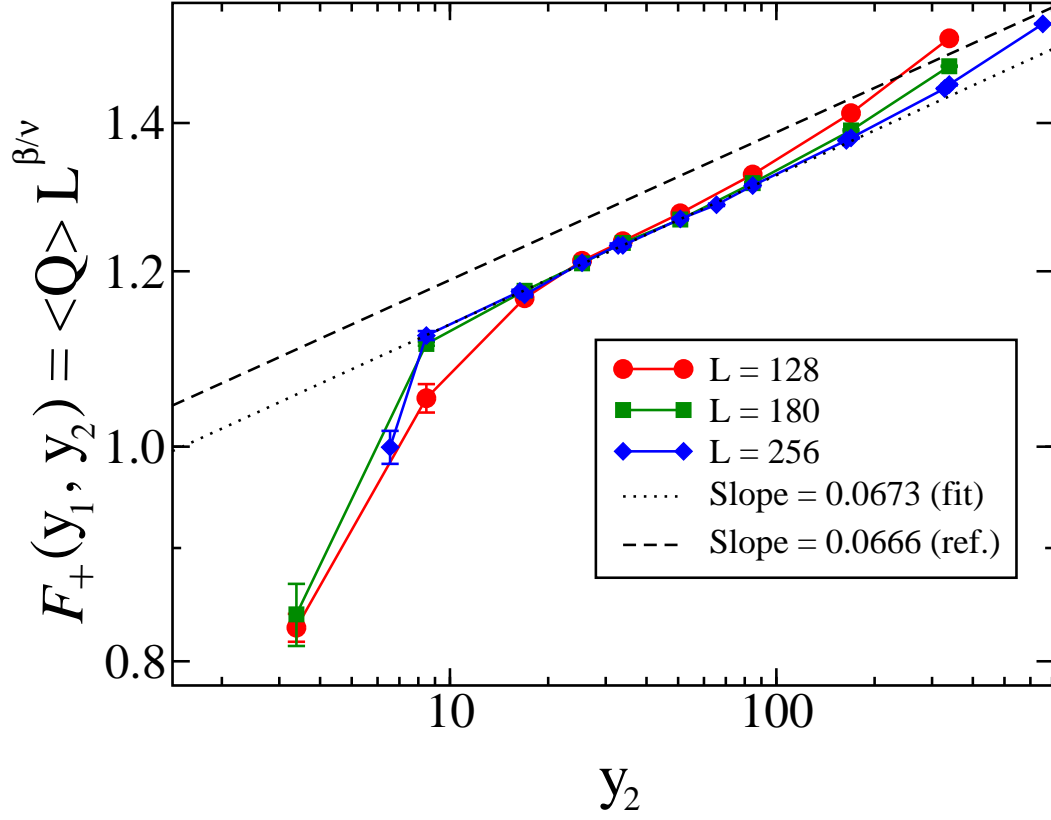
FIG. 2: (Color online.) Log-log plots of the scaling function $\mathcal{F}_+(y_1, y_2)$ vs y_1 for lattice sizes $L = 90, 128$, and 180. The values of y_1 plotted are 4.00, 17.2, 30.3, 43.4, 69.7, 147, and (in **(b)**) 280 and 477. **(a)** The data are shown for the values of y_2 listed on the plot. The best-fit line for the last five points of the $L = 180$ data at $y_2 = 3.39$, with slope -1.76 ± 0.07, is included along with a reference line with the slope $-\gamma_e = -1.75$. **(b)** The data for $y_2 = 3.39$ with two additional y_1 values illustrates the boundary of the regime of power-law scaling.
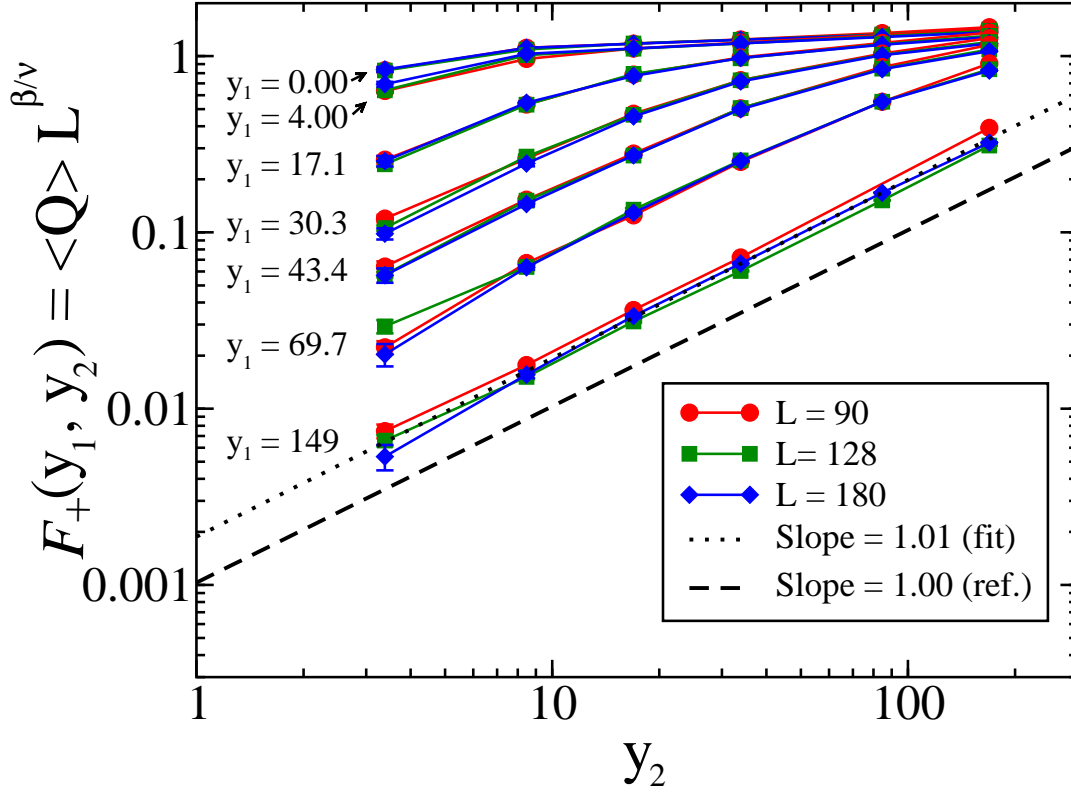
FIG. 3: (Color online.) Log-log plot of the scaling function $\mathcal{F}_+(y_1, y_2)$ vs $y_2 = (H_b/J)L^{\beta\delta/\nu}$ for lattice sizes $L = 90, 128$, and 180, for the constant values of y_1 labeled in the plot. The values of y_2 used are $y_2 = 3.39, 8.46, 16.9, 33.9, 84.6$, and 169. The dotted line represents the best fit to the first five points of the $L = 180$ data at $y_1 = 149$, and has a slope of 1.01 ± 0.01. The dashed line shows the slope value of 1, expected from Eq. (13).

FIG. 4: (Color online.) Log-log plot of the scaling function $\mathcal{F}_+(y_1, y_2)$ vs $y_2 = (H_b/J)L^{\beta\delta/\nu}$ for lattice sizes $L = 128$, 180, and 256, at the critical period P_c, where $y_1 = 0$. In the $L = 256$ data, near the values $y_1 = 16, 32, 165$, and 335, two closely spaced data points are actually plotted. The best-fit line to the $L = 256$ data in the range $8.46 < y_2 < 84.6$, shown as a dotted line in the plot, corresponds to a scaling exponent $1/\delta_{\mathrm{d}} = 0.0673 \pm 0.0008$. A reference line corresponding to scaling exponent $1/\delta_{\mathrm{e}} = 1/15 = 0.0666$ is also shown. These results are in complete agreement with those shown in Fig. 1.
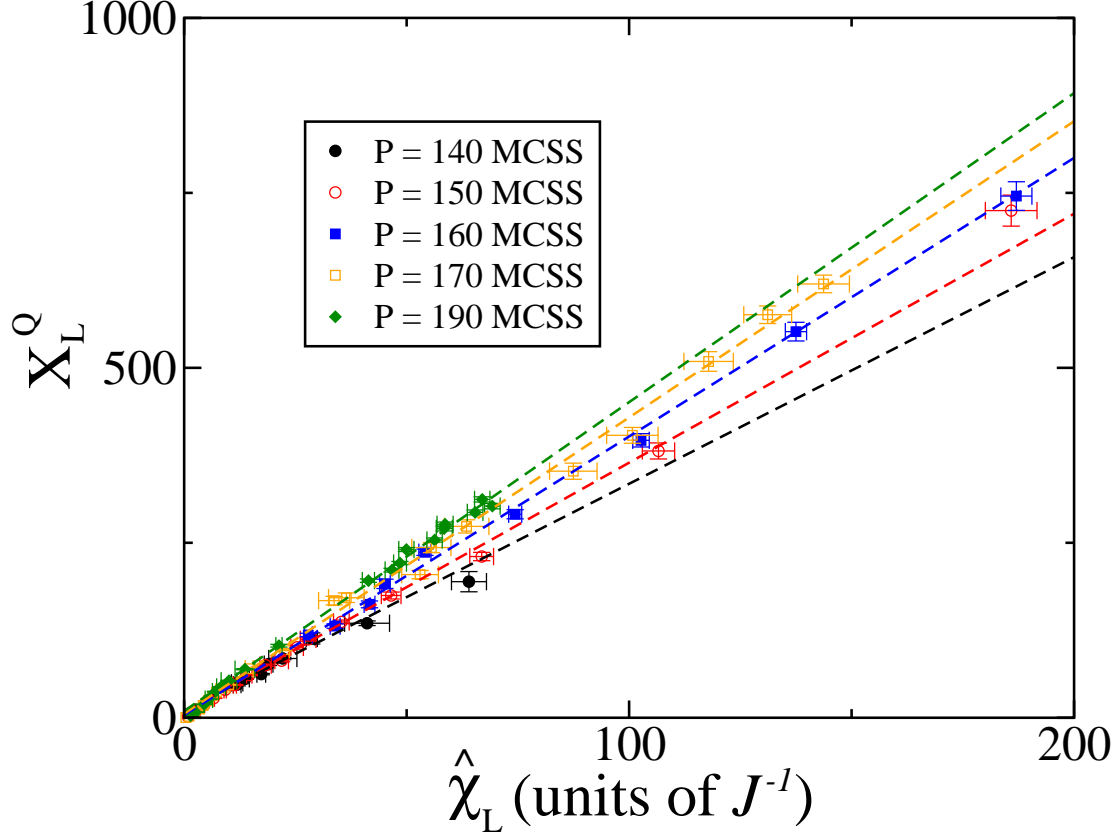
FIG. 5: (Color online.) The scaled fluctuations X_L^Q of the dynamic order paramater plotted vs its susceptibility $\hat{\chi}_L$ to the bias field H_b, calculated at $L = 180$, for periods $P = 140, 150, 160, 170$ and 190 MCSS. The quantity $\hat{\chi}_L$ was calculated using the numerical derivative in Eq. (17). The best-fit lines shown, whose slopes increase monotically with the period P of the data to which they were fit, were calculated as $(3.239J)\hat{\chi}_L + 10.42$, $(3.557J)\hat{\chi}_L + 8.735$, $(3.980J)\hat{\chi}_L + 3.889$, $(4.232J)\hat{\chi}_L + 5.868$ and $(4.497J)\hat{\chi}_L + 5.371$, respectively.
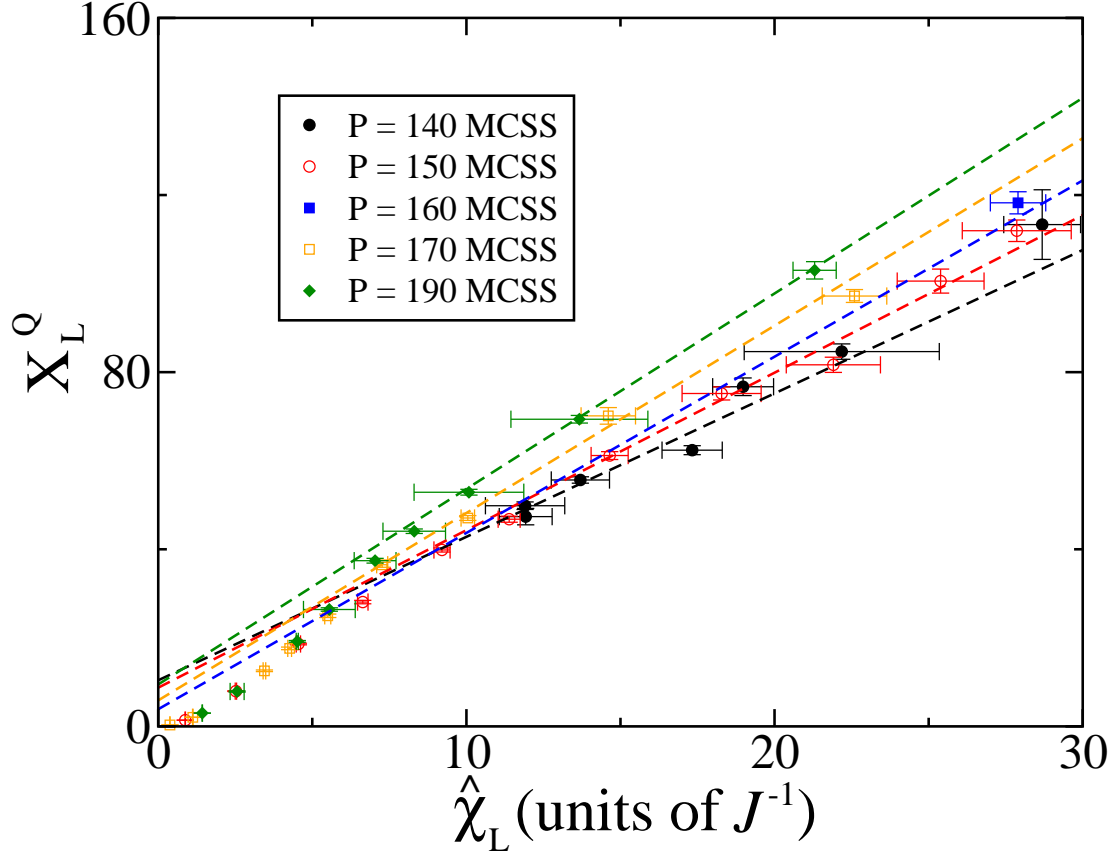
FIG. 6: (Color online.) Closeup of Fig. 5, showing the relationship of X_L^Q and $\hat{\chi}_L$ at low values of $\hat{\chi}_L$, which correspond to large values of the bias field H_b. For $P = 150$, 170 and 190 MCSS, data have been taken (and are shown) down to very low values of $\hat{\chi}_L$, where the breakdown of the linear relationship between X_L^Q and $\hat{\chi}_L$ can be clearly seen. The dashed lines are the same best-fit lines shown in Fig. 5.
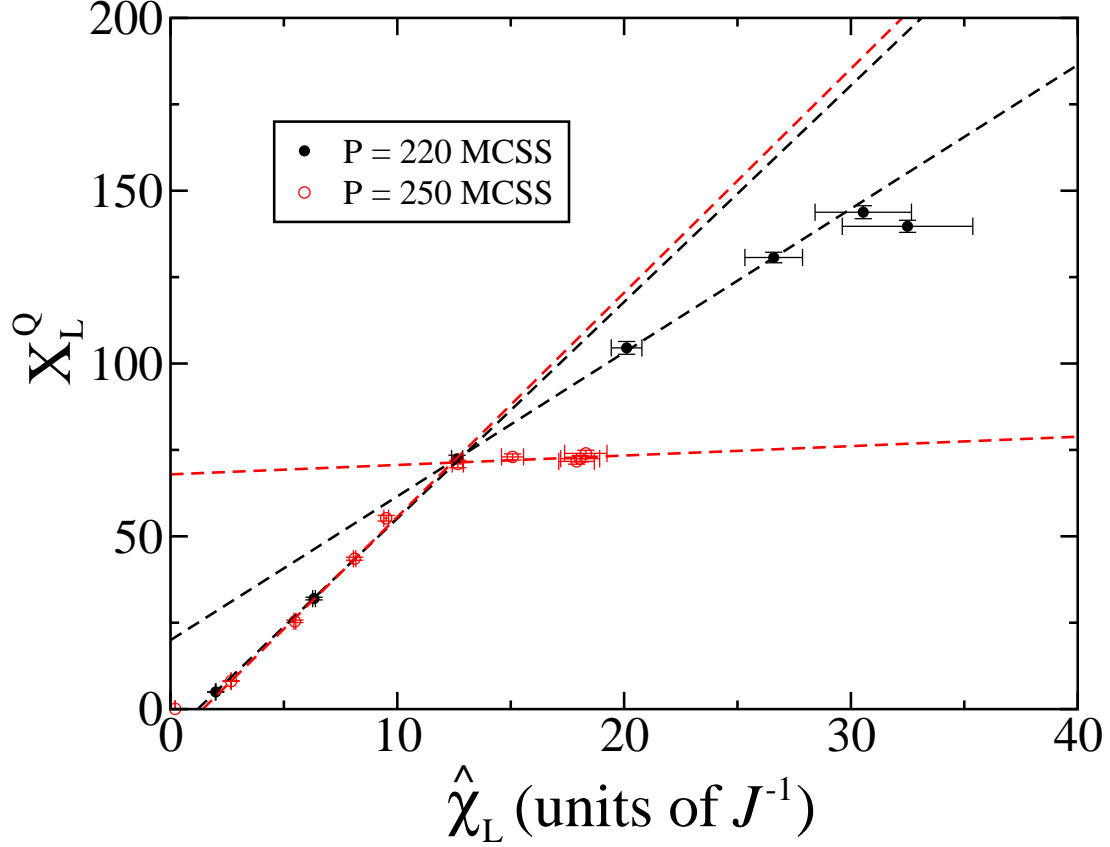
FIG. 7: (Color online.) The scaled fluctuations X_L^Q of the dynamic order paramater plotted vs its susceptibility $\hat{\chi}_L$ to the bias field H_b, calculated for lattice size $L = 180$, at periods $P = 220$ and 250 MCSS. At each period, the data were fit (purely phenomenologically) to two linear relationships. For $P = 220$ MCSS, the fits were calculated as $(6.265J)\hat{\chi}_L - 7.497$ at low $\hat{\chi}_L$, and $(4.161J)\hat{\chi}_L + 19.94$ at high $\hat{\chi}_L$. For $P = 250$ MCSS, the fits were $(6.485J)\hat{\chi}_L - 9.240$ at low $\hat{\chi}_L$, and $(0.2726J)\hat{\chi}_L + 67.92$ at high $\hat{\chi}_L$.
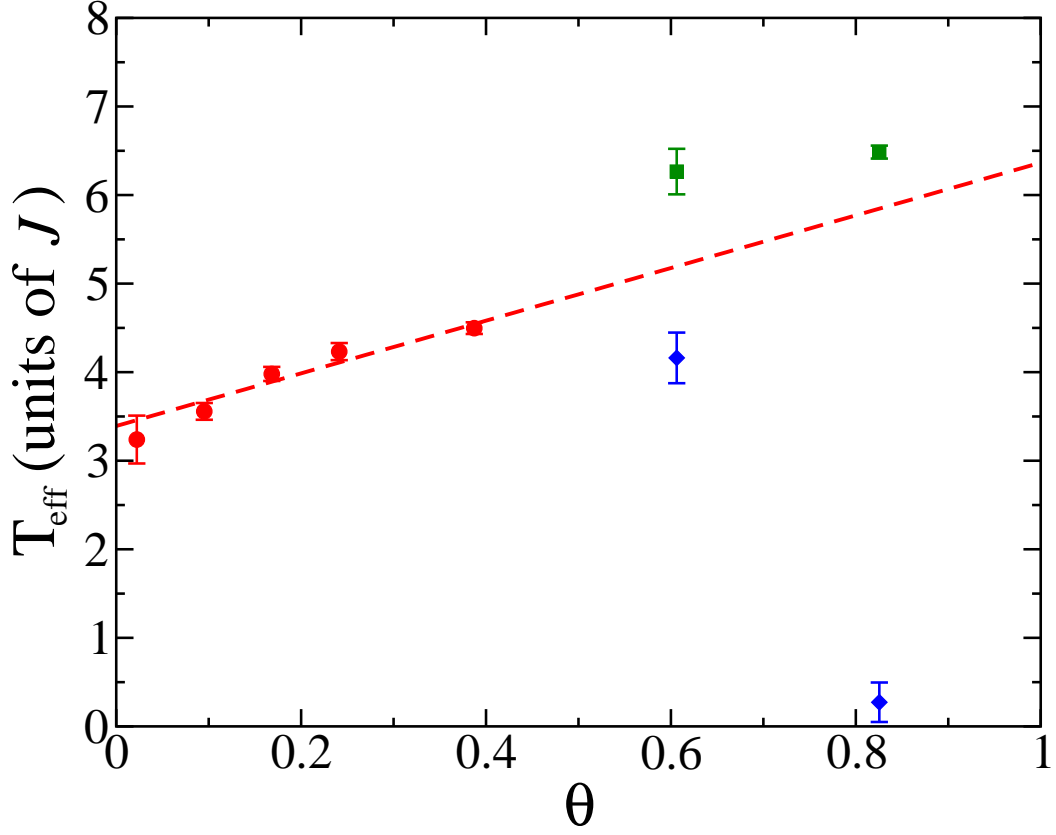
FIG. 8: (Color online.) The effective temperature T_{eff}, obtained as the slopes of the linear fits to the data in Figs. 5 and 7, plotted vs $\theta = (P - P_c)/P_c$. For the values $\theta = 0.606$ and 0.825 ($P = 220$ and 250 MCSS), the slopes of both linear regimes fit in Fig. 7 are plotted as T_{eff} values, using filled squares and diamonds rather than filled circles. The straight line is a weighted least-squares fit to the data below $\theta \approx 0.4$ ($P < 190$ MCSS), and has a slope of $2.97J$.
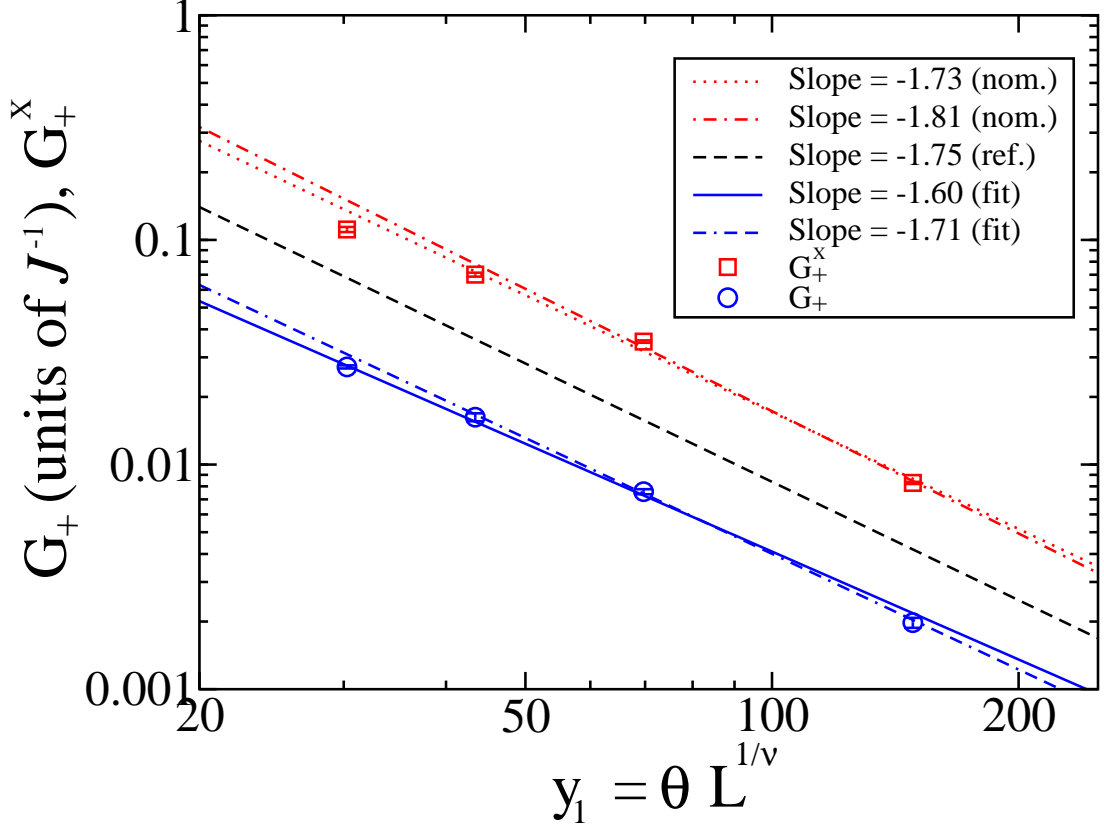
FIG. 9: (Color online.) Log-log plots of $\mathcal{G}_+(y_1, y_2)$ and $\mathcal{G}_+^X(y_1, y_2)$ vs y_1, over the range $y_1 = 30.3$ through 149, for $y_2 = 8.46$ at $L = 180$. The relatively small error bars on each data point can be seen inside the larger symbols. The solid and dash-dash-dotted lines are fits to all four and the last three $\mathcal{G}_+$ data points, respectively, and correspond to scaling exponents -1.60 ± 0.03 and -1.71 ± 0.05. The dotted and dash-dotted lines are the result of attempts to fit all four and the last three $\mathcal{G}_+^X$ data points, respectively. They correspond to nominal scaling exponents -1.73 ± 0.01 and -1.81 ± 0.02. The dashed line is a reference line corresponding to scaling exponent -1.75.
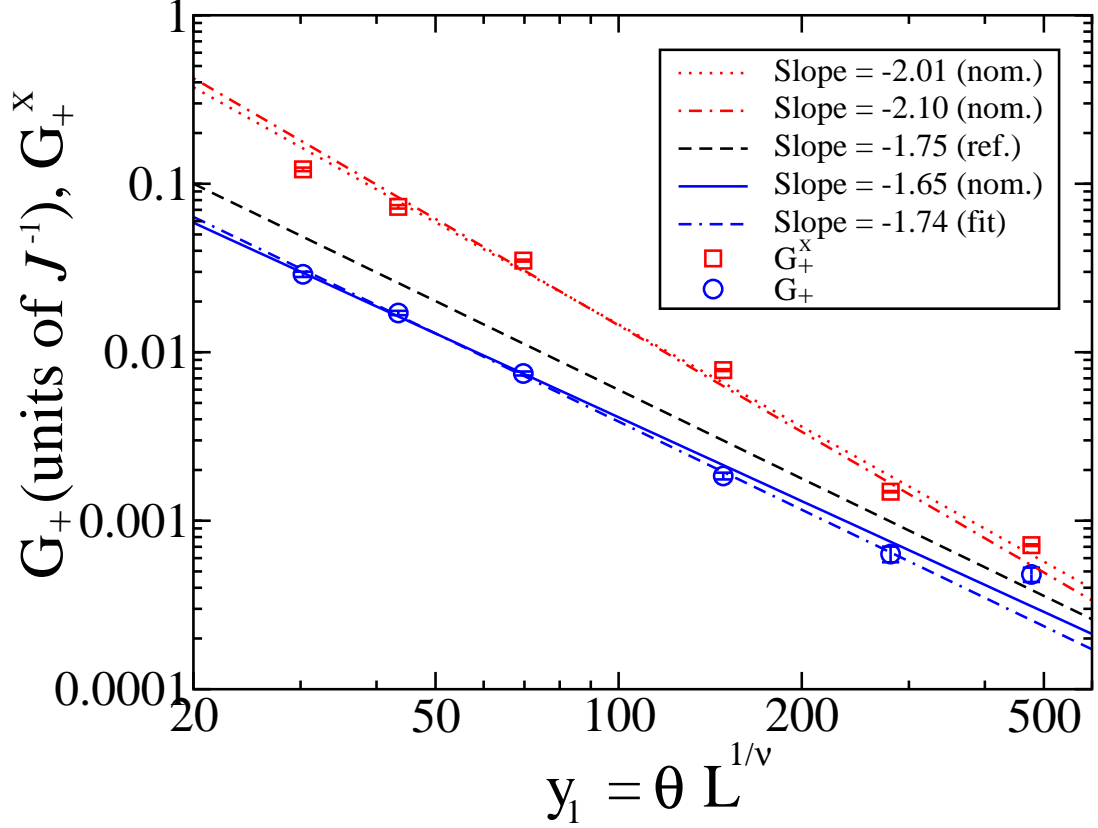
FIG. 10: (Color online.) Log-log plots of $\mathcal{G}_+(y_1, y_2)$ and $\mathcal{G}_+^X(y_1, y_2)$ vs y_1, over the range $y_1 = 30.3$ through 477, for $y_2 = 0$ at lattice size $L = 180$. The relatively small error bars on each data point can be seen inside the larger symbols. The solid and dash-dash-dotted lines show the result of attempts to fit all six and the first five $\mathcal{G}_+$ data points, and correspond to a nominal scaling exponent -1.65 ± 0.03, and a statistically significant scaling exponent -1.74 ± 0.03, respectively. The dotted and dash-dotted lines are the result of attempts to fit all six and the first five $\mathcal{G}_+^X$ data points, and correspond to nominal scaling exponents -2.01 ± 0.01 and -2.10 ± 0.01, respectively. The dashed line is a reference line corresponding to scaling exponent -1.75.
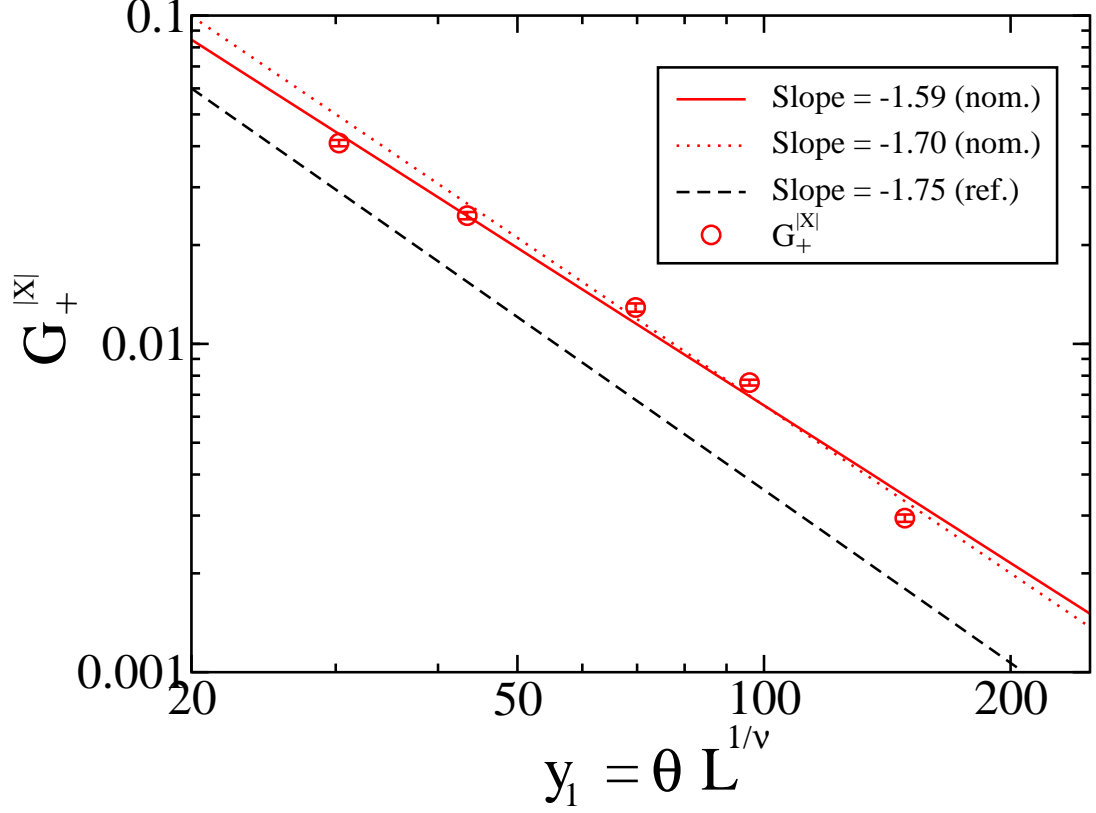
FIG. 11: (Color online.) Log-log plot of $\mathcal{G}_+^{|X|}(y_1, y_2)$ vs y_1, over the range $y_1 = 30.3$ through 149, for $y_2 = 0$ at lattice size $L = 180$. The relatively small error bars on each data point can be seen inside the larger symbols. The solid and dotted lines are the results of attempts to fit all five and the last four data points with a power-law relationship, and correspond to nominal scaling exponents of -1.59 ± 0.02 and -1.70 ± 0.03, respectively. The dashed line is a reference line corresponding to a scaling exponent of -1.75.
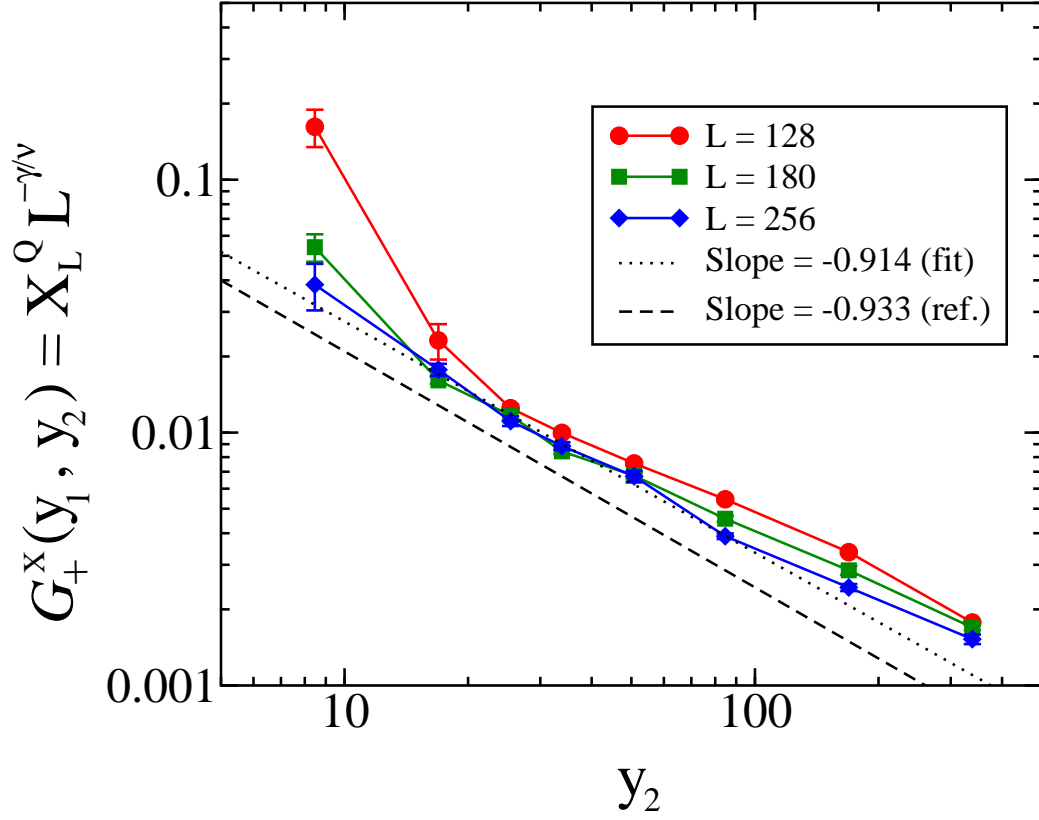
FIG. 12: (Color online.) Log-log plot of $\mathcal{G}_+^X(y_1, y_2)$ vs $y_2 = (H_b/J)L^{\beta\delta/\nu}$ for lattice sizes $L = 128$, 180, and 256, at the critical period P_c, where $y_1 = 0$. The best-fit line to the $L = 256$ data in the range $8.46 < y_2 < 84.6$, shown as a dotted line in the plot, corresponds to a scaling exponent $(1 - \delta_{\mathrm{d}})/\delta_{\mathrm{d}} = -0.914 \pm 0.029$. A reference line (dashed), corresponding to a scaling exponent $(1 - \delta_{\mathrm{e}})/\delta_{\mathrm{e}} = -14/15 \approx -0.933$, is also shown.